Green Chemistry

PAPER

View Article Online
View Journal | View Issue

Cite this: *Green Chem.*, 2026, **28**, 213

# Low indoor light-driven $CO_2$ conversion into visible $C_4$ bioplastic *via* homogeneous non-metal-based biohybrids under photoexcitation

Wenjing Wang, *[a] Mingzhi Zhang,[a] Meng Guo,[a] Jiaxin Wang,[a] Xuelian Wang,[a] Jianheng Yin,[a] Liang Chen[b] and Yaguang Li *[c]

Received 16th May 2025,
Accepted 10th November 2025

DOI: 10.1039/d5gc02437d

rsc.li/greenchem

The conversion of $CO_2$ into $C_4$ bioplastic through biohybrid systems comprising microorganisms and non-metal-based photocatalysts represents a promising strategy for high-value carbon utilization. However, existing non-metal-based biohybrids necessitate the addition of auxiliary agents or heterotrophic carbon sources due to the limited contact and interfacial mass transfer caused by the aggregation of photocatalysts and bacteria. In this work, a homogeneously autotrophic K/O co-doped g-$C_3N_4$ (K/O-CN) and *Ralstonia eutropha* (*R. eutropha*) biohybrid was developed to efficiently convert $CO_2$ into poly-β-hydroxybutyrate (PHB) without any auxiliary agents. Under low indoor light of 4000 lux (0.75 mW $cm^{-2}$), the K/O-CN–*R. eutropha* biohybrid achieved a PHB yield of $49.35 \pm 0.85$ mg $L^{-1}$ $d^{-1}$ surpassing non-metal-based biohybrids with added co-factors and reached a quantum efficiency of $5.88 \pm 0.16\%$ exceeding most metal-based biohybrids. The K/O co-doping changed stacked bulk layers to nanorods, which enveloped the bacterial cells with uniform dispersion, establishing a tight interaction, strong coupling, and effective electron transfer between them. Upon photoexcitation, K/O-CN catalyzed $H_2O$ splitting to generate $H_2$. Intracellularly, $H_2$ was oxidized to $H^+$, which participated in ATP synthesis and generated additional reducing equivalents (NADPH), thereby enhancing the carbon metabolic cycle and promoting the formation of key intermediates, ultimately driving the conversion of $CO_2$ to PHB. This work offers a streamlined and economically viable pathway for obtaining $C_4$ products from $CO_2$ and providing key insights into interfacial mass transfer and carbon metabolism changes within the biohybrid.

### Green foundation

1. Our work advances green chemistry by enabling efficient, additive-free $CO_2$-to-$C_4$ bioplastic (PHB) conversion under low indoor light using a novel photocatalyst/bacterium biohybrid. The process allows for simple one-step PHB extraction, supporting low-energy, renewable, and environmentally friendly $CO_2$ utilization.
2. This system achieved a PHB yield of $49.35 \pm 0.85$ mg $L^{-1}$ $d^{-1}$, surpassing non-metal-based biohybrids with added co-factors. The system uses a K/O-CN photocatalyst, which is non-toxic to microorganisms, ensuring biosafety and compatibility. Integrated with *R. eutropha*, a bacterium capable of self-replication, the system maintains high catalytic activity.
3. This system would become even greener when applied to large-scale $CO_2$ utilization and PHB production driven by widespread natural sunlight.

## 1. Introduction

Converting carbon dioxide into multi-carbon products enhances economic value and broadens the scope of carbon utilization. Artificial photocatalytic $CO_2$ reduction harnesses solar irradiation to activate photocatalysts for $CO_2$ conversion.[1,2] Numerous studies have employed strategies such as heterojunction construction,[3–7] composite formation,[8,9] and elemental doping[10] to enhance the $CO_2$ photoreduction performance of catalysts such as g-$C_3N_4$, achieving considerable progress. This approach can effectively convert $CO_2$ into $C_1$ and $C_2$,[11] while the efficiency and

---

[a] *College of Life Sciences, Engineering Research Center of Ecological Safety and Conservation in Beijing-Tianjin-Hebei (Xiong'an New Area) of MOE, Institute of Life Sciences and Green Development, Hebei University, Baoding 071002, China. E-mail: wangwenjing@hbu.edu.cn*

[b] *School of Energy, Power and Mechanical Engineering, North China Electric Power University, Baoding 071000, China*

[c] *Research Center for Solar Driven Carbon Neutrality, Engineering Research Center of Zero-carbon Energy Buildings and Measurement Techniques, Ministry of Education, The College of Physics Science and Technology, Hebei University, Baoding, 071002, China. E-mail: liyaguang@hbu.edu.cn*

selectivity for longer-chain products remain markedly low.[12,13] Natural carbon fixation of microorganisms offers a highly selective pathway for $CO_2$ conversion into multi-carbon products, yet its energy utilization efficiency is limited to 1%–3%.[14,15] The integration of artificial photocatalysis with microbial carbon fixation enables the multi-carbon conversion of $CO_2$ and augments the overall efficiency.[16–18] Currently, photocatalyst–microbe biohybrids, including CdS–*Methanosarcina barkeri*,[19] $Cd_{0.8}Zn_{0.2}S$–*Sporomusa ovata* (*S. ovata*),[20] CdS–*S. ovata*,[21] Zr-MOF–*Moorella thermoacetica* (*M. thermoacetica*),[22] and intracellular gold nanocluster–*M. thermoacetica*,[23] can convert $CO_2$ into value-added products such as $CH_4$, acetate, and acetic acid.[19–21,23] Photocatalyst–microbe biohybrids enable direct transfer between the photocatalyst and microbe within a single reactor, making the system integrated and reducing operational costs.

Poly-β-hydroxybutyrate (PHB, $C_4H_6O_2$) is a biodegradable plastic that offers a sustainable alternative to conventional petroleum-based plastics. In 2024, the global market size for bioplastics is estimated at approximately 2.09 million tons.[24] Converting $CO_2$ into PHB, valued at $4000–$6000 per ton,[25] presents a promising strategy for achieving high economic returns in carbon utilization. *Ralstonia eutropha* (*R. eutropha*) utilizes $CO_2$ for autotrophic growth, concurrently producing and accumulating hydrophobic PHB within its cytoplasm, which can be easily isolated and extracted. The existing methods to promote PHB production in *R. eutropha* primarily focus on optimizing culture conditions and genetic engineering. Compared with these methods, photocatalyst–*R. eutropha* biohybrids require simple operation with the incorporation of a photocatalyst and light to improve PHB production.

Few photocatalyst–*R. eutropha* biohybrids have been developed for PHB production from $CO_2$ using ZnSe/ZnS,[26] metal quantum dots,[27] $g\text{-}C_3N_4$-catalase,[28] or organic polymer dots.[29] It is still challenging to resolve the biotoxicity of metal photocatalysts and the need for auxiliary additives in non-metal systems to achieve an ideal PHB yield. Non-metal $g\text{-}C_3N_4$ with stable physicochemical properties and excellent biocompatibility[30,31] was used to construct hybrid systems aimed at PHB production. However, existing $g\text{-}C_3N_4$-based biohybrids primarily employ bulk $g\text{-}C_3N_4$ to construct a heterotrophic system utilizing fructose rather than $CO_2$ as the carbon source,[32] or a $g\text{-}C_3N_4$-catalase–*R. eutropha* system with additive $H_2O_2$-degrading enzymes.[28] The bulk $g\text{-}C_3N_4$ aggregates with bacterial cells hindering mass transfer at the abiotic–biotic interface. Furthermore, the changes of the overall metabolic profile and the intermediate metabolite in the biohybrids remain unclear.

To address these challenges, this study designs a uniformly dispersed $g\text{-}C_3N_4$–*R. eutropha* autotrophic biohybrid to efficiently drive $CO_2$ conversion to PHB without the need for any auxiliary agents under low indoor light irradiation. The system introduces nano-sized, scattered rod-like K/O co-doped $g\text{-}C_3N_4$ (K/O-CN) as a replacement for bulk $g\text{-}C_3N_4$, thereby increasing the interface contact and mass transfer at the abiotic–biotic interface. *R. eutropha* has a unique carbon metabolism pathway to utilize $CO_2$ to produce $C_4$ PHB and is capable of using $H_2$ as an electron donor, which makes it feasible to couple with the K/O-CN in a tandem system. In addition to assessing the final PHB product and coenzyme NADPH, this study conducts a comprehensive analysis of all metabolic intermediates and products within the biohybrid. The green-chemistry advancement of the K/O-CN–*R. eutropha* biohybrid lies in establishing a novel autotrophic, photo-driven paradigm for PHB production directly from $CO_2$, which operates without the need for any enzymes or electron mediators.

## 2. Materials and methods

### 2.1 Synthesis of PCN and K/O-CN

The melamine (99%), lithium chloride (LiCl, 99%), and potassium chloride (KCl, ≥99.5%) used in the synthesis of the photocatalyst were all supplied by Macklin Reagent Co., Ltd. The preparation procedure of K/O-CN is similar to that in the previous report.[33] The specific preparation procedure was as follows: 5 g of melamine was placed in a porcelain boat and calcined at 550 °C for 4 h in a tube furnace under air, with a heating rate of 5 °C $min^{-1}$. 1.90 g yellow pristine carbon nitride was obtained and denoted as PCN. Subsequently, 500 mg of PCN was thoroughly ground with 0.9 g of LiCl and 1.1 g of KCl in an agate mortar. The mixture was then placed in a porcelain boat and calcined at 550 °C for 4 h in a tube furnace under air, with a heating rate of 5 °C $min^{-1}$. After cooling to room temperature, 0.47 g calcined product was obtained, which was washed 5 times with boiling water and dried in a vacuum oven at 60 °C to obtain K/O-CN. To investigate the effect of doping amount, the co-doped samples were subjected to treatments with varying amounts of LiCl (0.74 g and 1.06 g) and KCl (0.9 g and 1.3 g) and accordingly designated as K/O-CN-1 and K/O-CN-2, respectively. Only K-doped $g\text{-}C_3N_4$ (K-CN) was prepared by calcining the PCN under an Ar atmosphere rather than in air. Only the O-doped $g\text{-}C_3N_4$ (O-CN) sample was prepared by calcining the PCN in air without the treatment with LiCl and KCl.

### 2.2 Cultivation of *R. eutropha* and construction of the photocatalytic biohybrid system

*R. eutropha* H16 (CGMCC 1.7092) was purchased from the China General Microbiological Culture Collection Center. The strain was sent to Sangon Biotech (Shanghai) Co., Ltd for identification, which confirmed it as *R. eutropha*. The relevant identification results are provided in Text S1. The composition of the culture media is detailed in Tables S1–S3. For the cultivation of microorganisms, the glycerol stock of *R. eutropha* stored at −80 °C was thawed and streaked onto a tryptic soy agar (TSA) plate, followed by incubation at 30 °C for 24 h in a constant temperature incubator. A well-grown single colony was then transferred into a tryptic soy broth (TSB) medium and cultured at 30 °C with shaking at 200 rpm under dark conditions for 24 h to enrich the culture. The bacterial culture was subsequently inoculated into a fructose medium at a 5%

inoculum volume and incubated at 30 °C with shaking at 200 rpm in the dark for 12 h.

For the construction of the biohybrid system, the fructose-pre-cultured bacterial suspension was centrifuged at 4 °C and 5000 rpm for 5 min to collect the bacterial cells. The cells were washed twice with a nitrogen-limited medium and then resuspended in 60 mL of nitrogen-limited medium containing various concentrations of K/O-CN (0.2–1 g $L^{-1}$), without K/O-CN, or with triethanolamine (TEOA, 5 g $L^{-1}$), ensuring an $OD_{600}$ of 0.2. The bacterial suspension was transferred into 100 mL serum bottles (height 5.31 cm, radius 2.45 cm). The bottles were evacuated and injected with a gas mixture ($N_2:H_2:CO_2:O_2$ = 76 : 10 : 10 : 4) until atmospheric pressure was reached. The obtained systems were incubated under autotrophic conditions at 30 °C with shaking at 200 rpm. During the photocatalytic process, the culture was exposed to light at an intensity of 4000 lux. The light was turned off under dark conditions. The light intensity was tuned in the range of 3000–5000 lux. For light–dark cycle experiments, the light and dark conditions were alternated every 12 h to achieve the desired cyclic conditions. For the photocatalytic long-term operation experiment of 6 d, 10 mL of samples were taken every 24 h to measure the PHB content. After sampling, 10 mL of fresh nitrogen-limited medium was added to the reactor. The reactor was then evacuated and purged with a $CO_2$-enriched mixed gas.

In the cyclic conditions, the biohybrid system after 48 h of cultivation was centrifuged to recover the photocatalyst, which was then thoroughly washed with deionized water and ethanol, dried, and subsequently reused in a new round of biohybrid reaction with the re-inoculation of *R. eutropha*. Owing to minor losses of the photocatalyst (approximately 15 wt%) during centrifugation and washing, a small amount of fresh K/O-CN was supplemented to maintain the optimal loading of 0.5 g $L^{-1}$ in the biohybrid system.

### 2.3 Detection of PHB

10 mL of cultured bacterial suspension was taken every 12 h and centrifuged at 10 000 rpm for 10 min. To maintain the atmosphere and ensure adequate $CO_2$ supply, after each 12 h sampling, the headspace of the reactor was first evacuated, and then a $CO_2$-containing gas mixture ($N_2:H_2:CO_2:O_2$ = 76 : 10 : 10 : 4) was refilled until atmospheric pressure was reached. The supernatant was discarded, and the cell pellet was washed twice with ultrapure water, followed by centrifugation to collect the cells. The collected cells were dried overnight at 55 °C. The dried cells were then transferred into a pressure-resistant thick-walled tube, and 2 mL of 3% sulfuric acid-acidified methanol and 2 mL of chloroform were added. The mixture was heated at 100 °C for 4 hours, with shaking every hour to ensure thorough cell disruption. After cooling to room temperature, 1 mL of distilled water was added to the tube, and the mixture was vigorously shaken for 1 min and then allowed to settle into layers. The chloroform layer was collected, filtered through a 0.22 μm syringe filter, and transferred into a screw-cap vial for gas chromatography analysis. The analysis was performed using a Fuli GC 9790 Plus II gas chromatograph with an RB-FFAP column and a flame ionization detector (FID). The separation and extraction of PHB are detailed in Text S2.

### 2.4 Physical, chemical, and biological characterization

The microstructural characterization was conducted using an FEI Nova Nano SEM 450 scanning electron microscope (SEM) and a Talos F200X transmission electron microscope (TEM) with an energy dispersive X-ray spectrometer (EDS) from Thermo Fisher Scientific. $N_2$ adsorption–desorption measurements were conducted on a Micromeritics ASAP 2460 to obtain the Brunauer–Emmett–Teller (BET) surface area and pore size distribution. X-ray diffraction (XRD) analysis was performed using a D-MAX 2500/PC X-ray diffractometer from Rigaku. Fourier-transform infrared (FTIR) spectroscopy was conducted using a Nicolet iS5 spectrometer from Thermo Fisher Scientific. Zeta potential measurements were conducted on a Malvern Zetasizer Nano ZS90 using water as the solvent. X-ray photoelectron spectroscopy (XPS) was carried out using a K-Alpha XPS system from Thermo Fisher Scientific. The potassium content in K/O-CN was determined by inductively coupled plasma optical emission spectroscopy (ICP-OES, PerkinElmer ICP 2100). $H_2$ production testing was performed in a 60 mL quartz reactor under xenon lamp irradiation, with specific conditions detailed in Text S3. The $H_2$ production test in nitrogen-limited culture medium was performed as detailed in Text S4. Ultraviolet–visible diffuse reflectance spectroscopy (UV-vis DRS) was performed using a UV-vis spectrometer (TU-1901) equipped with an integrating sphere from Beijing Persee. Electrochemical tests, including Mott–Schottky analysis, transient photocurrent response (TRP), electrochemical impedance spectroscopy (EIS), and linear sweep voltammetry (LSV), were conducted using a CHI 660E electrochemical workstation from Shanghai Chenhua, with specific conditions provided in Text S5. Photoluminescence (PL) spectra were recorded using an Edinburgh FLS980 spectrometer. For $^{13}CO_2$ isotope labeling experiment, $^{13}CO_2$ was used to replace $CO_2$ in the gas mixture and introduced into the reactor of K/O-CN–*R. eutropha* for PHB production. The culture was cultivated under 4000 lux light conditions for 48 h. PHB was then extracted from both K/O-CN–*R. eutropha* and K/O-CN–*R. eutropha* with $^{13}CO_2$ isotope labeling. The high-resolution solid-state $^{13}C$ Nuclear Magnetic Resonance (NMR) test was conducted for the extracted PHB using a Bruker AVANCE III 500 MHz by dissolving PHB in the solvent of $CDCl_3$ at 10 mg $ml^{-1}$.

The colony-forming units (CFU) were counted under an upright biological microscope of Nikon Ei. The optical density at a wavelength of 600 nm ($OD_{600}$) was measured daily using a UV-vis spectrometer (TU-1901) to monitor the growth of bacteria in the system. The NADPH/$NADP^+$ ratio, an indicator of the cellular redox state, was determined by analyzing 5 million cells from various systems grown in a nitrogen-limited medium for 48 h. The concentrations of NADPH and $NADP^+$ were measured using a coenzyme II NADPH content assay kit (MTT colorimetric method) from Solarbio Life Sciences, China, and the ratio was calculated. The $CO_2$ isothermal adsorption tests were performed at 25 °C on a Quantachrome Autosorb iQ from USA. Untargeted metabolomic analysis after 24 h illumination was performed at Paisenno Company using a Thermo Vanquish ultra-high-performance liquid chromatography (UHPLC) system coupled with a Thermo Orbitrap Exploris 120 mass spectrometer (Thermo Fisher Scientific, USA), under specific conditions outlined in Text S6. Multivariate dimensionality reduction analyses, including principal component analysis (PCA) and orthogonal partial least squares-discriminant analysis (OPLS-DA), were conducted using the R software package Ropls.

## 3. Results and discussion

### 3.1 Construction of the K/O-CN–*R. eutropha* biohybrid system

The K/O-CN–*R. eutropha* biohybrid system was constructed through a mixing-self-assembly approach (Fig. 1a). Initially, the bacteria were inoculated into a fructose medium to promote rapid growth and proliferation, thereby enriching the bacterial biomass. Subsequently, the enriched bacterial cells were introduced into an autotrophic medium containing K/O-CN, facilitating the mixing and self-assembly of the bacteria with K/O-CN. Under illumination, this biohybrid system was driven to catalyze the photoconversion of $CO_2$ into PHB. The morphology and composite state of the K/O-CN–*R. eutropha* biohybrid system were observed by SEM and TEM. After K/O co-doping treatment, the carbon nitride transformed from stacked blocky layers (Fig. S1 and S2) into nanorods (Fig. 1b and c). Based on $N_2$ adsorption–desorption measurements (Fig. S3a and b), K/O-CN exhibits a significantly larger specific surface area and pore volume than CN, providing more active sites and facilitating $CO_2$ adsorption and mass transport during the reaction. Uniform distributions of K and O were detected in K/O-CN as observed in TEM-EDS mapping (Fig. S4), indicating the successful co-doping of K and O. As shown in Fig. 1d and S5, K/O-CN combined with *R. eutropha* forms a uniformly dispersed composite system. In the biohybrid system, the *R. eutropha* cells maintained their original short rod-shaped structure, with the bacterial cells remaining

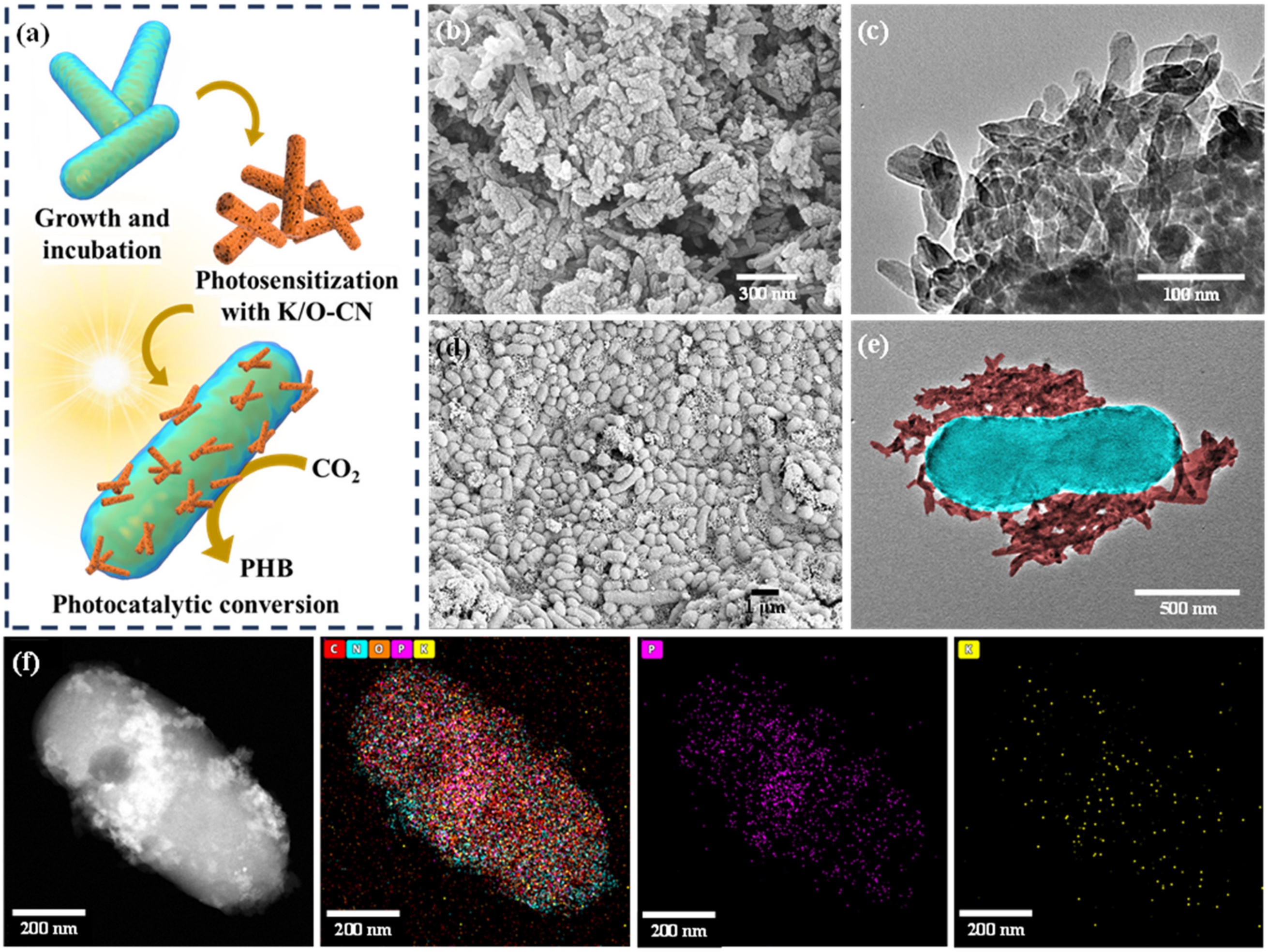

Fig. 1 Construction of the K/O-CN–*R. eutropha* biohybrid system. (a) Schematic illustration of the construction process, (b) SEM and (c) TEM images of K/O-CN, and (d) SEM, (e) TEM, and (f) TEM-EDS mapping images of the K/O-CN–*R. eutropha* biohybrid system.

intact. In the pure *R. eutropha* system, the bacterial surface appeared relatively smooth (Fig. S6 and S7), whereas in the biohybrid system, the nanorod-shaped K/O-CN surrounded the bacterial cells, establishing a close association (Fig. 1e, S8, and S9). TEM-EDS mapping of the biohybrid (Fig. 1f and S10) reveals the presence of common elements C, N, and O shared by both *R. eutropha* and K/O-CN, along with typical P element in *R. eutropha* and K element in K/O-CN. The uniform distribution of P and K substantiated the homogeneous integration of *R. eutropha* and K/O-CN. The homogeneous biohybrid with evenly distributed K/O-CN and *R. eutropha* enabled effective interaction and mass transfer between them.

A comparative analysis was conducted on the crystal structure, functional groups, and chemical states of K/O-CN, *R. eutropha*, and the K/O-CN–*R. eutropha* biohybrid. The XRD pattern of PCN (Fig. S11) exhibited a weak diffraction peak at 13.20° and a sharp diffraction peak at 27.40°, corresponding to the in-plane tri-s-triazine motifs ((100) planes) and the conjugated aromatic interlayer stackings ((002) planes), respectively. Similarly, K/O-CN also showed two main diffraction peaks. However, the peak for the (100) planes in K/O-CN shifted to a higher angle, around 14°, and the peak intensity of (002) planes reduced. These changes were attributed to the structural rearrangement and weakened interlayer stacking in K/O-CN due to the rod-like morphology induced by K/O doping.[34] Several low-intensity, broad diffraction peaks observed in K/O-CN were attributed to structural distortions or defects induced by the doping of K and O, which led to lattice distortions or the formation of localized amorphous phases within the CN matrix. In the XRD patterns (Fig. 2a), the K/O-CN–*R. eutropha* biohybrid exhibited three diffraction peaks, with the peak at 27.04° originating from the conjugated aromatic stacking of K/O-CN ((002) planes).[35] Additionally, two weak diffraction peaks at 13.32° and 16.78° overlapped with the corresponding structural peaks of *R. eutropha*, indicating the successful combination of K/O-CN and *R. eutropha*. For FTIR analysis (Fig. 2b), the K/O-CN–*R. eutropha* biohybrid showed a characteristic peak at 807 $cm^{-1}$, corresponding to the bending vibration of triazine units, while the peaks at 980 $cm^{-1}$ and 1650 $cm^{-1}$ corresponded to the skeletal vibrations of the CN heterocycles in K/O-CN.[36] Moreover, the biohybrid system exhibited characteristic peaks at 1060 $cm^{-1}$, 1450 $cm^{-1}$, and 1730 $cm^{-1}$, corresponding to C–C bending, C–H bending, and C═O stretching vibrations, respectively. The peaks in the range of 3020–2890 $cm^{-1}$, assigned to the stretching vibrations of C–H groups, originated from *R. eutropha*. The biohybrid system thus retains the characteristic functional groups of both K/O-CN and *R. eutropha* without the appearance of new peaks, indicating the absence of new chemical bond formation. Meanwhile, zeta potential measurements in Fig. S12 indicated that the surfaces of K/O-CN and *R. eutropha* both carried negative charges, suggesting that their interaction was unlikely to be driven by electrostatic attraction. Excluding chemical bonding and electrostatic forces, it could be inferred

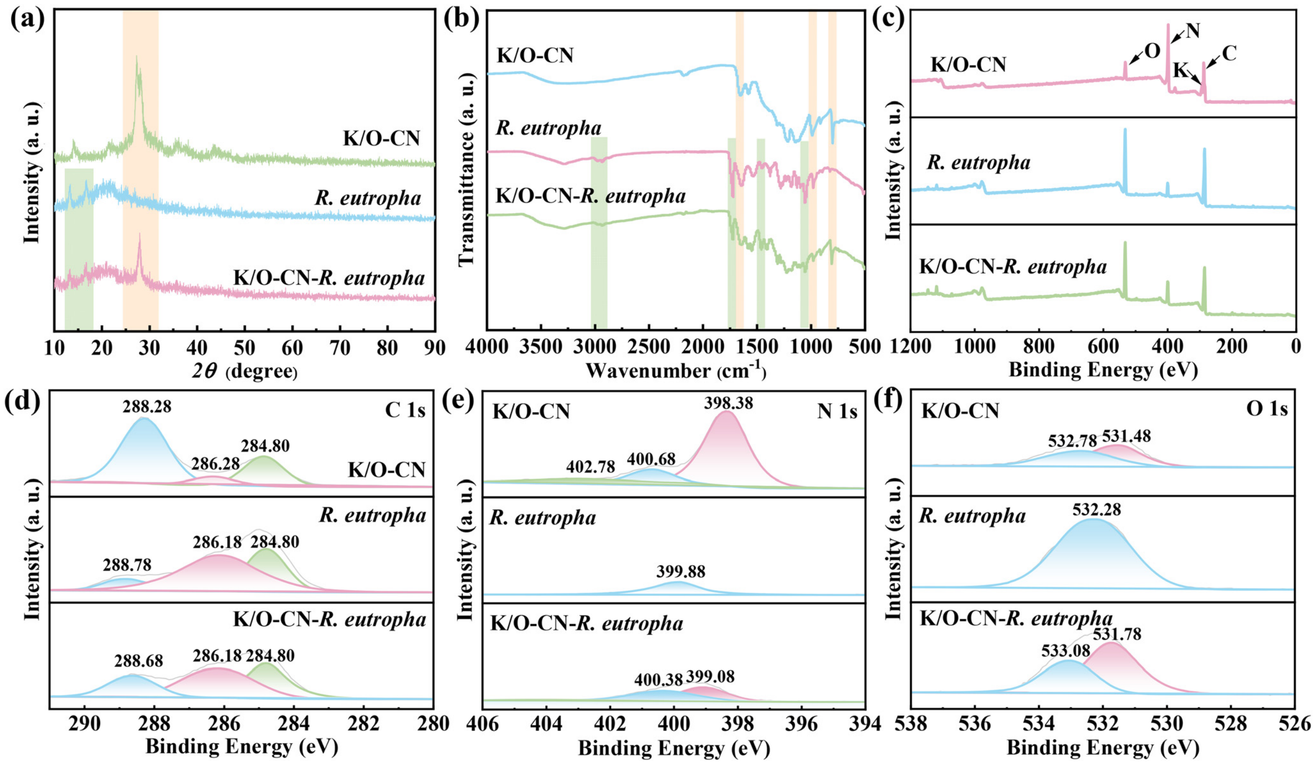

**Fig. 2** Physical and chemical characterization studies of the K/O-CN–*R. eutropha* biohybrid. (a) XRD patterns, (b) FTIR spectra, (c) XPS survey spectra, (d) C 1s high-resolution XPS spectra, (e) N 1s high-resolution XPS spectra, and (f) O 1s high-resolution XPS spectra.

that K/O-CN and *R. eutropha* interacted through intermolecular forces, specifically van der Waals interactions, between the surface of the photocatalyst and biomolecules.

Based on XPS survey analysis in Fig. 2c, K/O-CN, *R. eutropha* and the biohybrid were primarily composed of the elements C, N, and O, with a small amount of K present in K/O-CN. The atomic percentages of K and O in K/O-CN were found to be 2.25 at% and 7.73 at%, confirming the successful co-doping of K and O. The ICP-OES analysis revealed that the K content in K/O-CN was 1.80 wt%, in good agreement with the value determined by XPS. No Li element was detected in K/O-CN in the XPS survey scan. Meanwhile, no distinct peak was observed in the Li 1s high-resolution spectrum of K/O-CN (Fig. S13). These results indicated that Li element was totally removed from K/O-CN during the process of boiling water cleaning. For the C 1s XPS spectrum (Fig. 2d), the pure bacterial system showed three component peaks ascribed to C═O (288.78 eV), C–N (286.18 eV), and C═C (284.80 eV).[37,38] After forming the biohybrid with K/O-CN, the C═O peak in the biohybrid shifted to 288.68 eV,[39] moving toward lower binding energy and higher intensity. In the N 1s XPS spectrum (Fig. 2e), unlike the isolated peak of *R. eutropha*, the biohybrid system showed two fitted peaks with binding energies close to those of K/O-CN. Compared to K/O-CN, the peak corresponding to tertiary N ($N–C_3$) in the biohybrid shifted negatively to 400.38 eV, while the peak corresponding to C–N═C shifted positively to 399.08 eV.[33] The O 1s XPS spectrum (Fig. 2f) reveals that the C–O and C═O peaks in the biohybrid system shifted towards higher binding energies compared to those in K/O-CN, indicating electron loss by K/O-CN during its interaction with *R. eutropha*. The analysis of these chemical states suggested that there were contact and interactions between K/O-CN and *R. eutropha* in the biohybrid system. The K 2p high-resolution XPS spectrum of K/O-CN was also recorded, as shown in Fig. S14. The results showed that K/O-CN exhibited two characteristic peaks at 293.00 eV and 295.60 eV, corresponding to the coordination of $K^+$ with nitrogen atoms in the imide groups of carbon nitride and nitrogen atoms in other nitrogen-containing groups, respectively.

### 3.2 Photocatalytic performance of $CO_2$ to PHB conversion

$H_2$ production tests indicate that the $H_2$ production performance of K/O-CN was 2.73 times that of PCN (Fig. S15). Compared to the original PCN, K/O-CN had a broader light absorption range (Fig. S16a and b), a narrower bandgap (Fig. S17a and b), and a higher reduction potential (Fig. S18 and S19). Electrochemical and PL tests indicate that K/O-CN also had higher efficiency in charge carrier migration and separation (Fig. S20 and S21) and lower charge transfer resistance (Fig. S22) than PCN. These benefits contributed to its enhancement for $H_2$ production performance. K/O-CN exhibited higher $H_2$ production and better photocatalytic performance than K/O-CN-1 with less K-doping, K/O-CN-2 with higher K-doping, K-CN, and O-CN (Fig. S23). Moreover, as shown in Fig. S24, the pure culture medium did not produce $H_2$, while the system with K/O-CN was able to stably generate $H_2$ under 4000 lux illumination. When the K/O-CN–*R. eutropha* biohybrid was introduced, the $H_2$ production decreased compared with the system with K/O-CN, indicating that the biohybrid consumed the $H_2$ generated by K/O-CN during photocatalytic water splitting. When PCN was replaced with K/O-CN and combined with *R. eutropha* to construct a biohybrid system, the $CO_2$ conversion capability of the system was improved (Fig. S25). The PHB yield in K/O-CN–*R. eutropha* increased by 45% compared to that in PCN–*R. eutropha*. The extraction and detection processes of the PHB product are described in Text S2 in the SI and section 2.3. These methods effectively extracted PHB and allowed for accurate quantification of its content.

To determine the carbon source and the purity of PHB, $^{13}CO_2$ isotope labeling experiment and high-resolution solid-state $^{13}C$ NMR test were conducted. The $^{13}C$ NMR results in Fig. S26 and S27 showed that both PHB from K/O-CN–*R. eutropha* and K/O-CN–*R. eutropha* with $^{13}CO_2$ exhibited characteristic $^{13}C$ resonances at 168.1, 76.1–66.7, 39.9, and 19.8 ppm, corresponding to the C═O, CH, $CH_2$, and $CH_3$ structural units,[40] respectively, which aligned with the typical structure of PHB. No obvious additional impurity peaks were observed, indicating that the extracted PHB was of high purity. Different from the weak resonance signals for most structural units in the PHB from K/O-CN–*R. eutropha*, the resonance peaks of structural units significantly increased in the PHB from K/O-CN–*R. eutropha* with $^{13}CO_2$. This indicated that the incorporation of $^{13}C$ isotopes from $^{13}CO_2$ into PHB enhanced its abundance, suggesting that K/O-CN–*R. eutropha* had produced PHB from $CO_2$.

Fig. 3a explores the optimal concentration of K/O-CN for the biohybrid system. Compared to the pure bacterial system, the addition of K/O-CN within the range of 0.2–1 g $L^{-1}$ enhanced the PHB yield. The maximum accumulation of PHB was achieved with a K/O-CN concentration of 0.5 g $L^{-1}$. TEM results showed that the biohybrid with a low K/O-CN concentration (0.2 g $L^{-1}$) did not sufficiently interact with the bacteria (Fig. S28a). At high concentrations of K/O-CN (1 g $L^{-1}$) in the biohybrid, an excess of photocatalyst aggregated on the bacterial surface (Fig. S28b), which inhibited the bacteria's absorption and utilization of nutrients from the culture medium. To eliminate the influence of carbon from K/O-CN, the PHB production of the biohybrid without supplementing $CO_2$ ($N_2 : H_2 : O_2 = 86 : 10 : 4$) was tested as shown in Fig. S29. The results indicated that the PHB yield was 0 under these conditions, suggesting that the biohybrid was unable to utilize the carbon from K/O-CN for PHB synthesis. The addition of the sacrificial agent TEOA (5 g $L^{-1}$) resulted in a moderate increase in PHB yield, but the enhancement was limited (Fig. S30). The limited improvement caused by TEOA addition was due to its potential biotoxicity and the intrinsic metabolic constraints of the bacteria, which prevented further enhancement of PHB synthesis despite the increased electron supply. Considering cost and energy efficiency, the focus remained on research within the sacrificial agent-free system.

Fig. 3b illustrates the impact of light exposure on the PHB production of the K/O-CN–*R. eutropha* biohybrid. Under low

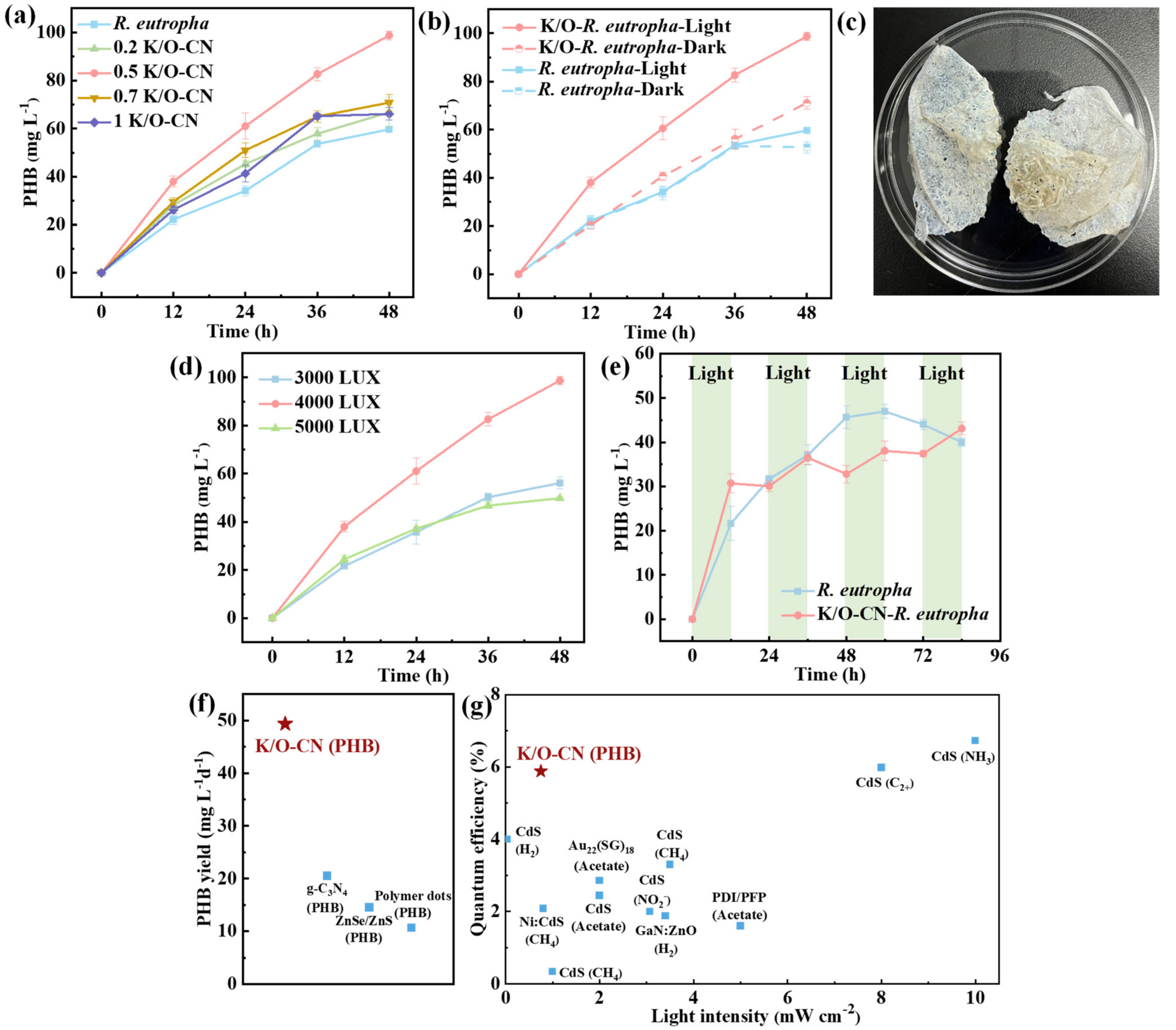

**Fig. 3** Photocatalytic performance of $CO_2$ to PHB conversion by K/O-CN–*R. eutropha* biohybrids (each test was repeated 3 times to obtain the average and standard deviation). (a) Photocatalytic PHB yields by the biohybrids with various amounts of K/O-CN (0.2–1 g $L^{-1}$) and *R. eutropha*, (b) PHB yields by the K/O-CN (0.5 g $L^{-1}$)–*R. eutropha* biohybrid and *R. eutropha* under dark and light-exposure conditions, (c) crude PHB extracted from the biohybrid cultured for 48 h, (d) photocatalytic PHB yields by the K/O-CN (0.5 g $L^{-1}$)–*R. eutropha* biohybrid under different light intensities (3000–5000 lux), (e) PHB yields by the K/O-CN (0.5 g $L^{-1}$)–*R. eutropha* biohybrid and *R. eutropha* under a light–dark cycle with a 12 h time interval, (f) comparison of the PHB production yield from $CO_2$ with autotrophic *R. eutropha*, and (g) comparison of the quantum efficiency in different photocatalytic biohybrid systems (all carbon utilization systems can use $CO_2$ as the carbon source).

indoor light irradiation (4000 lux, 0.75 mW $cm^{-2}$), the PHB yield of the K/O-CN–*R. eutropha* biohybrid reached 49.35 ± 0.85 mg $L^{-1}$ $d^{-1}$, representing a 65% increase compared to the pure bacterial system without K/O-CN (29.85 ± 0.25 mg $L^{-1}$ $d^{-1}$). This enhancement is huge for the natural carbon metabolism pathway for PHB production. This suggests that the system can greatly improve the efficiency of $CO_2$ utilization, reduce production costs, and accelerate the industrialization of PHB. In the dark, the PHB production of the biohybrid system was similar to that of the pure bacterial system, indicating that the enhancement in $CO_2$ conversion within the biohybrid system was light-dependent. The biohybrid cultured for 48 h was subjected to a single separation and extraction to yield crude PHB, as shown in Fig. 3c. At a light intensity of 4000 lux, the PHB yield of the biohybrid system was significantly higher than that at other light intensities, representing the optimal illumination conditions (Fig. 3d). At illumination intensities below 4000 lux, the light is insufficient to effectively activate the photocatalyst. However, when the light intensity was too high, it generated excessive reactive oxygen species (ROS) from the photocatalyst, which surpassed the bacteria's antioxidant capacity and caused oxidative stress.[41]

The photosynthetic behavior of the K/O-CN–*R. eutropha* biohybrid system was studied using a 12 h light–dark cycle (Fig. 3e). Throughout the light–dark cycle, the PHB accumulation in the biohybrid system exhibited an increasing trend and was higher than that in the pure bacterial system. During light exposure, the PHB content in the biohybrid system showed significant accumulation, whereas in the dark, there was a slight decrease in PHB levels due to the bacteria utilizing PHB as an energy source to sustain growth.[42] For the pure *R. eutropha*, the accumulation of PHB was not influenced by light. The PHB production of *R. eutropha* initially increased and then decreased over time in 96 h, with the decrease being attributed to the depletion of nutrients and the reduction in bacterial growth rate. Due to the continuous alteration of cultivation conditions, which affected bacterial activity and metabolism, the K/O-CN–*R. eutropha* biohybrid did not exhibit a significant advantage over the *R. eutropha* system in terms of PHB yield under light–dark conditions. This also indicated that the performance of the biohybrid was light-dependent. The K/O-CN–*R. eutropha* biohybrid was compared with reported photocatalytic biohybrid systems. For PHB production, the K/O-CN–*R. eutropha* surpassed non-metal autotrophic biohybrids with added co-factors (Fig. 3f and Table S4). The PHB productivity of the K/O-CN–*R. eutropha* biohybrid was markedly higher than that of the *g*-$C_3N_4$-based microbial electrosynthesis (MES) system (20.31 mg $L^{-1}$ $d^{-1}$),[43,44] while it also simplified the reaction configuration and significantly reduced operational costs. The quantum efficiency (QE) of K/O-CN–*R. eutropha* reached 5.88 ± 0.16%, as calculated using Eqn (1)–(3) (Text S7), which exceeded most metal-based biohybrids (Fig. 3g and Table S5).

We conducted a long-term operation of the K/O-CN–*R. eutropha* biohybrid system for 6 d in Fig. S31. The results showed that the maximum PHB accumulation occurred between 48 and 72 h, after which the PHB content began to decline. This observation aligns with the typical growth pattern of *R. eutropha*, which includes the lag phase, exponential phase, stationary phase, and death phase. In the cyclic text (Fig. S32), the PHB yield of the biohybrid system in 48 h after three consecutive cycles of K/O-CN reuse remained above 92.23% of the initial value. Furthermore, XRD and FTIR analyses of K/O-CN before and after the reactions (Fig. S33) confirmed that its crystalline structure and surface functional groups remained unchanged, indicating excellent structural stability and recyclability. Overall, these results demonstrate that K/O-CN in the biohybrid system can be readily separated and effectively reused through a simple recovery process. Therefore, to maximize the PHB yield, rather than long-term operation, the K/O-CN–*R. eutropha* biohybrid system should be operated for 48 h and then reactivated by re-inoculation and photocatalyst addition.

### 3.3 Main characteristic analysis of the K/O-CN–*R. eutropha* biohybrid

The CFU (Fig. 4a and S34) of K/O-CN–*R. eutropha* and PCN–*R. eutropha* presented the same near-linear increase as the pure bacterial system, indicating that the addition of K/O-CN and PCN did not affect the bacterial growth status, and both K/O-CN and PCN were non-toxic and exhibited good biocompatibility. The CFU assays of K/O-CN–*R. eutropha* with various amounts of K/O-CN (0.2–1 g $L^{-1}$) presented a similar increasing trend over time, implying that the K/O-CN amount in a suitable range did not affect bacterial activity (Fig. S35). OD measurements were also conducted to monitor bacterial growth. However, the presence of K/O-CN increased light absorption and the optical density, leading to higher OD values for the K/O-CN–*R. eutropha* system. Therefore, OD testing in Fig. S36 was only used as a supplementary experiment to reflect the overall trend. The $OD_{600}$ values of both the biohybrid and pure bacterial systems showed an upward trend, indicating continuous bacterial accumulation in both systems. The TPR was used to test the generation and separation characteristics of photo-generated electron–hole pairs in the system (Fig. 4b). Under light, the K/O-CN–*R. eutropha* biohybrid generated photocurrents, demonstrating that it possessed light-excitation properties. The photocurrent intensity of the biohybrid system was higher than that of pure K/O-CN, demonstrating that the combination with *R. eutropha* had gen-

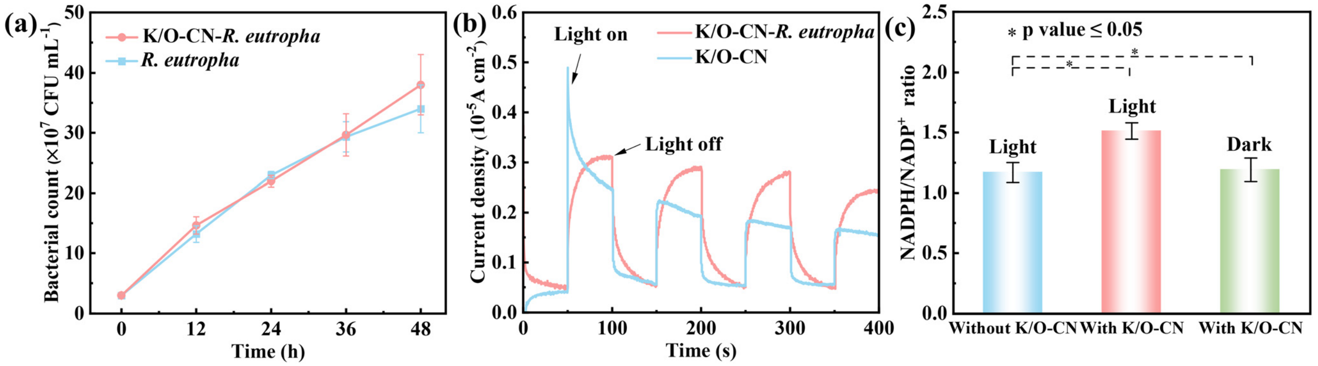

**Fig. 4** Main characteristic analysis of the K/O-CN–*R. eutropha* biohybrid. (a) CFU assays (each test was repeated 3 times to obtain the average and standard deviation), (b) TPR test, and (c) intracellular NADPH/$NADP^+$ ratio (each test was repeated 3 times to obtain the average and standard deviation).

erated more charge carriers and improved the electron–hole separation efficiency. Notably, the photocurrent of the biohybrid exhibited a curved rather than square-wave response, primarily because the presence of microorganisms altered the charge transfer kinetics of the system. Specifically, the microbial membranes and biomacromolecules slowed down electron transfer and introduced capacitive effects. Compared to pure K/O-CN, the biohybrid system showed a reduced charge transfer resistance (Fig. S37) and increased current density (Fig. S38). The incorporation of the bacteria facilitated charge transfer within the system and accelerated the separation of electron–hole pairs. The $CO_2$ adsorption capacity of the K/O-CN–*R. eutropha* biohybrid, K/O-CN, and *R. eutropha* was tested (Fig. S39). The results indicated that the $CO_2$ adsorption capacity of the K/O-CN–*R. eutropha* biohybrid (4.21 $cm^3$ $g^{-1}$) was significantly higher than that of pure *R. eutropha* (0.84 $cm^3$ $g^{-1}$). This enhancement was attributed to the K/O-CN, which possessed a rod-like porous nanostructure, resulting in a higher $CO_2$ adsorption capacity (9.66 $cm^3$ $g^{-1}$). The improved $CO_2$ adsorption capacity of the K/O-CN–*R. eutropha* biohybrid enabled efficient capture and utilization of $CO_2$.

During the Calvin–Benson–Bassham (CBB) cycle for PHB production by *R. eutropha*, NADPH is utilized as a reducing equivalent. Based on this, the NADPH/$NADP^+$ ratio (Fig. 4c) and NADPH quantity (Fig. S40) were measured for both the biohybrid and pure bacterial systems. Under illumination, the NADPH/$NADP^+$ ratio of the K/O-CN–*R. eutropha* system is 1.51, which was higher than that of the pure bacterial system under light (1.17) and the biohybrid system in the dark (1.19). The combined effects of K/O-CN addition and light exposure enhanced the NADPH/$NADP^+$ ratio in the biohybrid system. The NADPH quantity in the K/O-CN–*R. eutropha* system under light (0.054 nmol $10^{-4}$ cell) was higher than that in both the pure bacterial system under light and the biohybrid system in the dark. These results suggest that the photogenerated electrons from K/O-CN under light were transferred from the extracellular to the intracellular receptors, generating additional NADPH and promoting the energy metabolism of *R. eutropha*, which in turn increases PHB production.

To investigate the $CO_2$ metabolic pathways and changes in metabolic products, untargeted metabolomic analysis was performed on both the biohybrid and pure bacterial systems after illumination. A total of 596 metabolites were identified in both systems, with organic heterocyclic compounds representing the largest proportion (22.3%, Fig. S41). The principal metabolic product, PHB, belongs to this category, which was consistent with the macroscopic experimental results. PCA (Fig. 5a) and OPLS-DA (Fig. S42) score plots indicated that the biohybrid and pure bacterial systems were distributed in different quadrants, with significant metabolic differences, demonstrating that the introduction of K/O-CN under light had a substantial impact on the bacterial metabolic state. Volcano plot analysis (Fig. 5b) showed that many metabolites were upregulated and downregulated in the biohybrid system compared to the pure bacterial system. The types of upregulated metabolites (134) were significantly more than those of downregulated metabolites (40), indicating enhanced metabolism in the biohybrid system. Further analysis of differential metabolites revealed changes related to cell metabolism and PHB production, as shown in Fig. 5c. In the biohybrid system, amino acids such as L-threonine, lysine, and histidine were significantly upregulated, promoting protein synthesis and cell metabolic growth. The increase in ornithine, a participant in one-carbon metabolism, facilitated this process. The rise in phosphate and adenosine monophosphate (AMP) supported the synthesis of cellular energy currency, adenosine triphosphate (ATP). An increase in Nicotinamide Adenine Dinucleotide (NAD), an electron carrier, accelerated intracellular redox reactions. The increase in glyceraldehyde-3-phosphate, a metabolic intermediate, promoted the generation of reducing power (NADPH). The content of acetyl-CoA, a core intermediate in cellular metabolism and PHB synthesis, directly determined the PHB yield.[45] The acetyl-CoA content of the biohybrid system was 6.56 times that of pure bacteria. The increase in 3-hydroxybutyric acid, a monomer of PHB, confirmed the increased PHB yield within the biohybrid system.

### 3.4 Mechanism of photocatalytic $CO_2$ to PHB conversion

A comparative summary of key parameters for biohybrid and pure bacterial systems (Fig. 6a) reveals that the K/O-CN–*R. eutropha* biohybrid exhibited superior overall performance. The incorporation of K/O-CN led to several advantages: (1) it was non-toxic and exhibited good biocompatibility; (2) it increased the $CO_2$ adsorption capacity; (3) it generated additional reducing equivalents, enhancing bacterial energy metabolism; (4) it facilitated the production of key metabolic intermediates such as acetyl-CoA. These combined benefits significantly enhanced the K/O-CN–*R. eutropha* system's ability to utilize $CO_2$ and produce PHB.

In summary, the effect of K/O co-doping on PCN involved the following points: (1) after K/O co-doping treatment, the morphology of PCN changed from stacked bulk layers to nanorods; (2) the $H_2$ production performance of K/O-CN was 2.73 times that of PCN; (3) compared to PCN, K/O-CN exhibited a broader light absorption range, a narrower bandgap, and higher reduction potential; (4) K/O-CN showed a smaller charge transfer resistance and higher photogenerated carrier mobility and separation efficiency compared to PCN. Furthermore, the effects of K/O co-doping on the biohybrid for photocatalytic $CO_2$ conversion were reflected in several aspects: (1) the nanorod morphology of K/O-CN prevented the photocatalyst from aggregating into agglomerates with the bacteria, facilitating the effective combination of K/O-CN and *R. eutropha*; (2) K/O-CN provided more $H_2$ to *R. eutropha* than PCN, driving *R. eutropha* to utilize $CO_2$ for PHB production; (3) the $CO_2$ conversion capability of the K/O-CN–*R. eutropha* biohybrid was improved compared to the PCN–*R. eutropha* hybrid.

Both photocatalytically generated $H_2$ and injected $H_2$ participated in cellular metabolism and PHB biosynthesis. In the absence of injected $H_2$ ($N_2 : CO_2 : O_2 = 86 : 20 : 4$), the cells perished and no PHB was produced (Fig. S43), indicating that

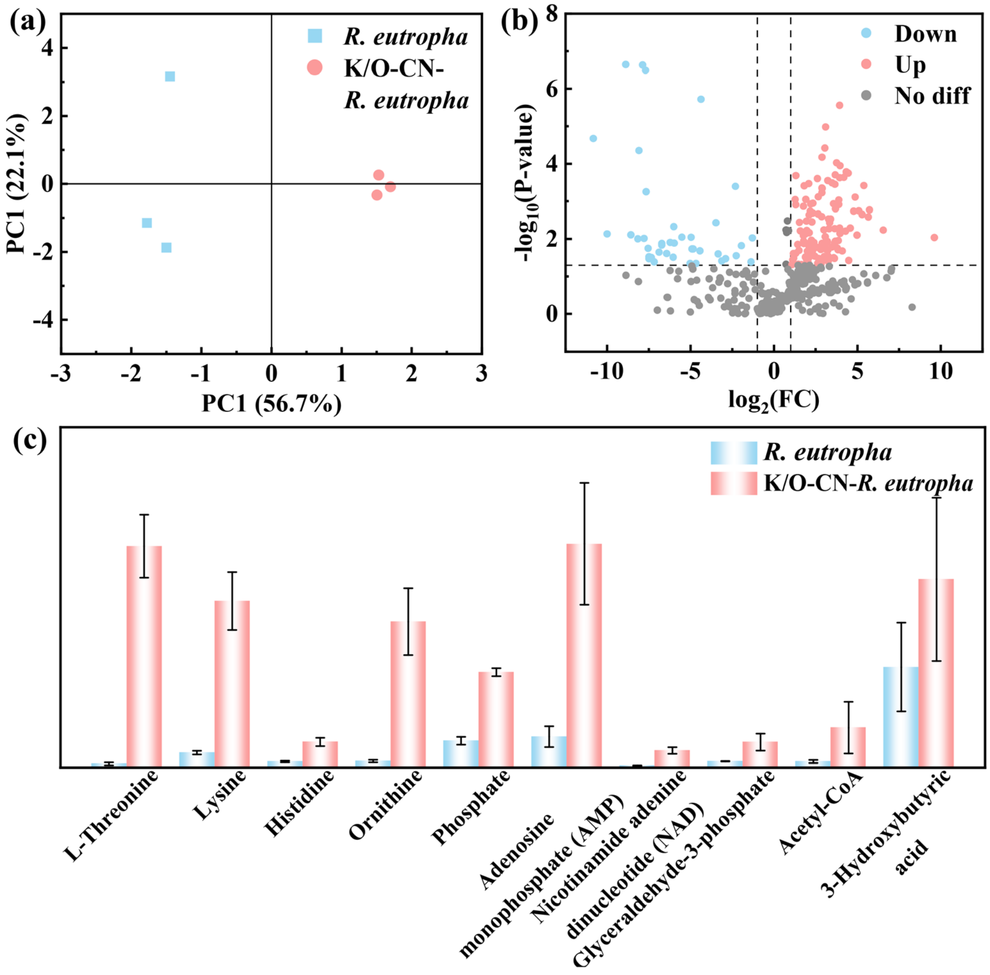

**Fig. 5** Metabolome analysis of the K/O-CN–*R. eutropha* biohybrid and *R. eutropha* groups (each group involved three biological replicates). (a) PCA score plots, (b) volcano plots of metabolites (up, upregulation, fold change (FC) > 1 and *p* value <0.05; down, downregulation, FC < 1 and *p* value <0.05; no diff, no difference of significance), and (c) relative abundance comparison of influential metabolites.

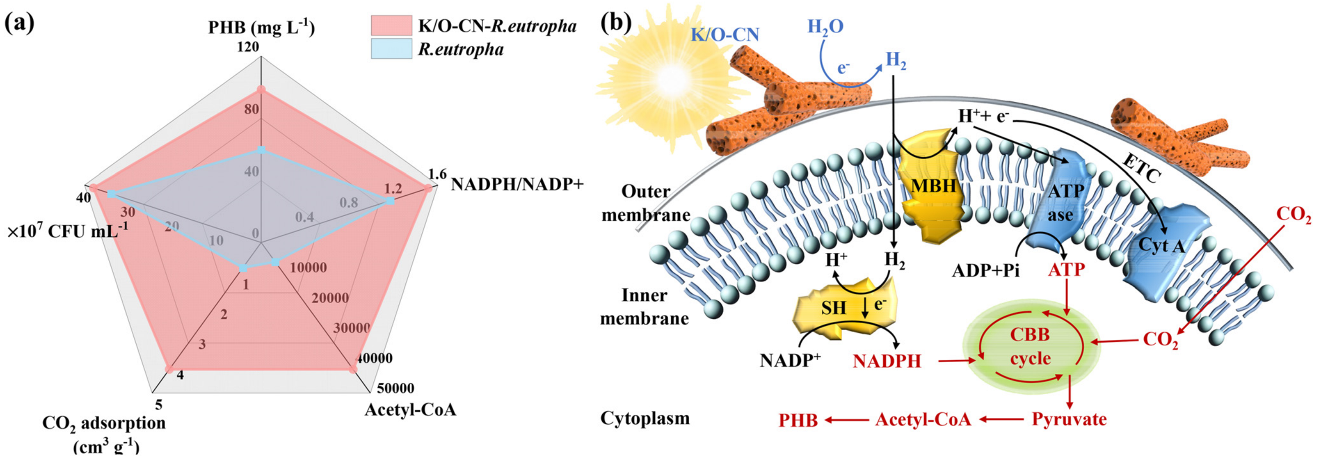

**Fig. 6** Proposed mechanism of photocatalytic $CO_2$ to PHB conversion in the K/O-CN–*R. eutropha* biohybrid system. (a) Comparison of the main characteristics between K/O-CN–*R. eutropha* and *R. eutropha* and (b) illustration of $CO_2$ to PHB conversion and charge transfer in the K/O-CN–*R. eutropha* biohybrid (MBH, membrane-bound hydrogenase; SH, soluble hydrogenase; ATPase, adenosine triphosphatease; ETC, electron transport chain; Cyt A, cytochrome oxidase; CBB, Calvin–Benson–Bassham cycle).

injected $H_2$ served as an essential energy source for maintaining cell survival and metabolism. Concurrently, the photocatalytic $H_2$ was rapidly utilized by the bacteria as an *in situ* source of reducing power and energy for PHB biosynthesis with the upregulation of ATP-related metabolites and NADPH levels.

The mechanism underlying the light-driven K/O-CN–*R. eutropha* biohybrid for $CO_2$ fixation and PHB biosynthesis, along with the mass and charge transfer processes at the abiotic–biotic interface, is elucidated in Fig. 6b. Upon photoexcitation, K/O-CN generates electron–hole pairs, which undergo redox reactions splitting $H_2O$ to produce $H_2$. The evolved $H_2$ diffuses into the cell, where a portion is captured by membrane-bound hydrogenase (MBH) located in the inner membrane, catalyzing its oxidation into protons ($H^+$) and electrons ($e^-$). The $H^+$ contributes to ATP synthesis, while the $e^-$ enters the electron transport chain (ETC). Another portion of $H_2$ diffuses into the cytoplasm, where soluble hydrogenase (SH) oxidizes it into $H^+$ and $e^-$, driving the reduction of $NADP^+$ to NADPH. ATP and NADPH subsequently function as the energy source and reducing agent, respectively, within the CBB cycle for $CO_2$ fixation. Through a series of metabolic intermediates such as pyruvate and acetyl-CoA, $CO_2$ is ultimately converted into PHB. Without light or a photocatalyst, a small amount of $H_2$ dissolved in the culture medium is utilized by *R. eutropha*. It is oxidized *via* MBH and SH into $H^+$ and $e^-$, contributing to ATP and NADPH synthesis and facilitating the conversion of $CO_2$ into PHB.

Based on the inherent metabolic pathways of *R. eutropha*, the utilization of $H_2$ without light or a photocatalyst is similar to that under light conditions. The key difference lies in the fact that, under light, the $H_2$ generated from water splitting by K/O-CN is utilized, whereas, in the dark, *R. eutropha* relies on $H_2$ dissolved in the culture medium. Under light conditions, the observed elevation in ATP-related metabolites, the increased $NADPH/NADP^+$ ratio, and the accumulation of key intermediates such as acetyl-CoA and 3-hydroxybutyrate validate that $H_2$ generated from the water splitting by K/O-CN promotes the $CO_2$-to-PHB conversion efficiency in this biohybrid system.

## 4. Conclusions

This work presents a design of a uniformly autotrophic K/O-CN–*R. eutropha* biohybrid, capable of driving the efficient conversion of $CO_2$ into visible $C_4$ bioplastic without any auxiliary agents. In this system, rod-shaped K/O-CN surrounded the bacterial cells and bound closely with them, thereby increasing the contact of the abiotic–biotic interface. The strong interactions between K/O-CN and *R. eutropha* facilitated the mass transfer across the interface. Under low indoor light of 4000 lux (0.75 mW $cm^{-2}$), the K/O-CN–*R. eutropha* hybrid achieved a PHB yield of 49.35 ± 0.85 mg $L^{-1}$ $d^{-1}$, outperforming non-metal composite systems with the presence of additives. The quantum efficiency of the K/O-CN–*R. eutropha* system reached 5.88 ± 0.16%, exceeding that of most metal-based biohybrids. The incorporation of K/O-CN in constructing the biohybrid exhibited good biocompatibility, augmented the quantity and separation efficiency of photo-generated charge carriers, produced additional reducing equivalents, and promoted the biosynthesis of key metabolic intermediates such as acetyl-CoA. Upon photoexcitation, K/O-CN decomposed $H_2O$ to generate $H_2$, which was subsequently oxidized to participate in ATP synthesis and drive the generation of reducing equivalents like NADPH, thereby accelerating the carbon metabolic cycle and efficiently converting $CO_2$ into high-value PHB.

## Author contributions

Wenjing Wang: conceptualization, project administration, writing – original draft, and funding acquisition. Mingzhi Zhang: investigation and writing – original draft. Meng Guo: investigation and writing – original draft. Jiaxin Wang: investigation and visualization. Xuelian Wang: data curation and investigation. Jianheng Yin: data curation and investigation. Liang Chen: methodology and funding acquisition. Yaguang Li: supervision, writing – review and editing.

## Conflicts of interest

There are no conflicts to declare.

## Data availability

The data that support the findings of this study are available from the corresponding author.

Supplementary information (SI) is available. See DOI: https://doi.org/10.1039/d5gc02437d.

## Acknowledgements

This work was supported by the National Natural Science Foundation of China (52306135, 52106141), the Science Research Project of Hebei Education Department (BJK2022054), the Natural Science Foundation in Interdisciplinary Research of Hebei University (DXK202109), and the Advanced Talents Incubation Program of Hebei University (521000981377).

## References

1 R. T. Chen, Z. F. Ren, Y. Liang, G. H. Zhang, T. Dittrich, R. Z. Liu, Y. Liu, Y. Zhao, S. Pang, H. Y. An, C. W. Ni, P. W. Zhou, K. L. Han, F. T. Fan and C. Li, *Nature*, 2022, **610**, 296–301.

2 K. Sun, Y. Huang, Q. Y. Wang, W. D. Zhao, X. S. Zheng, J. Jiang and H.-L. Jiang, *J. Am. Chem. Soc.*, 2024, **146**, 3241–3249.

3 G. dos Santos, L. Tian, R. Gonçalves, H. García and L. Rossi, *Adv. Funct. Mater.*, 2025, **35**, 2422055.

4 J. Cruz, G. Silva, E. Dias, D. Lima, J. Torres, P. Silva and C. Ribeiro, *ACS Appl. Mater. Interfaces*, 2024, **17**, 13029–13036.

5 M. F. Lu, Q. Q. Li, C. L. Zhang, X. X. Fan, L. Li, Y. M. Dong, G. Q. Chen and H. F. Shi, *Carbon*, 2020, **160**, 342–352.

6 Y. B. Zhong, H. B. Zhu, X. M. Xie, L. Yang, Y. J. Shen, Q. W. Fan, Z. B. Xie and Z. G. Le, *Inorg. Chem.*, 2025, **64**, 2706–2715.

7 H. L. Chen, F. Y. Liu, Y. Y. Lin, Z. Zuo, W. T. Wu, Q. Qi, Z. Peng, D. Zou and C. C. Chen, *Mater. Today Sustainability*, 2023, **23**, 100430.

8 J. Park, H. Liu, G. Piao, U. Kang, H. W. Jeong, C. Janáky and H. Park, *Chem. Eng. J.*, 2022, **437**, 135388.

9 P. Zhang, N. Li, L. Li, Y. Yu, R. Tuerhong, X. Su, B. Zhang, L. Han and Y. Han, *ChemPhysChem*, 2024, **25**, e202400075.

10 Z. Chen, G. Ding, Z. Wang, Y. Xiao, X. Liu, L. Chen, C. Li, H. Huang and G. Liao, *Adv. Funct. Mater.*, 2025, **35**, 2423213.

11 L. Wang, Y. Qi, Z. Yang, H. Wu, J. Liu, Y. Tang and F. Wang, *Green Energy Resour.*, 2023, **1**, 100036.

12 Y. X. Xu, J. L. Qin, F. Wang and H. Z. Wang, *Green Chem.*, 2025, **27**, 4489–4503.

13 A. Kumar and R. Ananthakrishnan, *Green Chem.*, 2020, **22**, 1650–1661.

14 S. Cestellos-Blanco, H. Zhang, J. M. Kim, Y.-X. Shen and P. D. Yang, *Nat. Catal.*, 2020, **3**, 245–255.

15 X. Fang, S. Kalathil and E. Reisner, *Chem. Soc. Rev.*, 2020, **49**, 4926–4952.

16 K. K. Sakimoto, A. B. Wong and P. D. Yang, *Science*, 2016, **351**, 74–77.

17 J. Ye, C. Wang, C. Gao, T. Fu, C. H. Yang, G. P. Ren, J. Lü, S. G. Zhou and Y. J. Xiong, *Nat. Commun.*, 2022, **13**, 6612.

18 G. Y. Liu, F. Gao, C. Gao and Y. J. Xiong, *Chem Catal.*, 2021, **1**, 1367–1377.

19 J. Ye, J. Yu, Y. Y. Zhang, M. Chen, X. Liu, S. G. Zhou and Z. He, *Appl. Catal., B*, 2019, **257**, 117916.

20 K. J. Zhang, R. J. Li, J. X. Chen, L. Y. Chai, Z. Lin, L. Zou and Y. Shi, *Appl. Catal., B*, 2024, **342**, 123375.

21 Y. He, S. R. Wang, X. Y. Han, J. Y. Shen, Y. W. Lu, J. Z. Zhao, C. P. Shen and L. Qiao, *ACS Appl. Mater.*, 2022, **14**, 23364–23374.

22 Z. Ji, H. Zhang, H. Liu, O. M. Yaghi and P. D. Yang, *Proc. Natl. Acad. Sci. U. S. A.*, 2018, **115**, 10582–10587.

23 H. Zhang, H. Liu, Z. Q. Tian, D. L. Lu, Y. Yu, S. Cestellos-Blanco, K. K. Sakimoto and P. D. Yang, *Nat. Nanotechnol.*, 2018, **13**, 900–905.

24 T. R. Sun, J. J. L. Guzman, J. D. Seward, A. Enders, J. B. Yavitt, J. Lehmann and L. T. Angenent, *Nat. Commun.*, 2021, **12**, 4119.

25 S. Price, U. Kuzhiumparambil, M. Pernice and P. Ralph, *J. Environ. Chem. Eng.*, 2022, **10**, 107502.

26 Y. H. Feng, M. Y. Xu, P.-L. Tremblay and T. Zhang, *Int. J. Hydrogen Energy*, 2021, **46**, 21901–21911.

27 Y. C. Ding, J. R. Bertram, C. Eckert, R. R. Bommareddy, R. Patel, A. Conradie, S. Bryan and P. Nagpal, *J. Am. Chem. Soc.*, 2019, **141**, 10272–10282.

28 P.-L. Tremblay, M. Y. Xu, Y. M. Chen and T. Zhang, *iScience*, 2020, **23**, 100784.

29 W. Yu, M. V. Pavliuk, A. Liu, Y. Zeng, S. P. Xia, Y. M. Huang, H. T. Bai, F. T. Lv, H. N. Tian and S. Wang, *ACS Appl. Mater. Interfaces*, 2022, **15**, 2183–2191.

30 X. C. Wang, K. Maeda, A. Thomas, K. Takanabe, G. Xin, J. M. Carlsson, K. Domen and M. Antonietti, *Nat. Mater.*, 2009, **8**, 76–80.

31 C. Y. Feng, J. Luo, C. L. Chen, S. W. Zuo, Y. F. Ren, Z. P. Wu, M. Hu, S. Ould-Chikh, J. Ruiz-Martínez, Y. Han and H. B. Zhang, *Energy Environ. Sci.*, 2024, **17**, 1520–1530.

32 M. Y. Xu, P.-L. Tremblay, L. L. Jiang and T. Zhang, *Green Chem.*, 2019, **21**, 2392–2400.

33 W. Liu, P. F. Wang, J. Chen, X. Gao, H. Che, B. Liu and Y. H. Ao, *Adv. Funct. Mater.*, 2022, **32**, 2205119.

34 Y. Pang, P. Li, X. Ma, L. Sun, Y. Liu, D. Qu, L. An and Z. Sun, *EES Catal.*, 2023, **1**, 810–831.

35 Y. Xia, Z. H. Tian, T. Heil, A. Y. Meng, B. Cheng, S. W. Cao, J. G. Yu and M. Antonietti, *Joule*, 2019, **3**, 2792–2805.

36 L. Chen, J. Y. Yu, Z. Y. Lyu, X. Y. Wen, Y. F. Wang, S. H. Cao and W. Wang, *Appl. Surf. Sci.*, 2024, **642**, 158550.

37 Z. Wei, M. L. Liu, Z. J. Zhang, W. Q. Yao, H. W. Tan and Y. F. Zhu, *Energy Environ. Sci.*, 2018, **11**, 2581–2589.

38 Q. Fan, H. Zhang, D. Liu, C. Yan, H. Zhu, Z. Xie and Z. Le, *J. Org. Chem.*, 2023, **88**, 7391–7400.

39 Q. Fan, D. Liu, Z. Xie, Z. Le, H. Zhu and X. Song, *J. Org. Chem.*, 2023, **88**, 14559–14570.

40 P. Ravindran and N. Vasanthan, *Macromolecules*, 2015, **48**, 3080–3087.

41 J.-Y. Zeng, X.-S. Wang, X.-H. Liu, Q.-R. Li, J. Feng and X.-Z. Zhang, *Natl. Sci. Rev.*, 2023, **10**, nwad142.

42 M. S. Morlino, R. Serna García, F. Savio, G. Zampieri, T. Morosinotto, L. Treu and S. Campanaro, *Biotechnol. Adv.*, 2023, **69**, 108264.

43 K. Zhang, X. Xu, X. L. Li, T. Song, J. Xie and T. Guo, *Fuel*, 2024, **357**, 129740.

44 M. R. Galih Pangestu, S. A. Razzak and S. Uddin, *Green Energy Resour.*, 2025, **3**, 100131.

45 F. Pietrocola, L. Galluzzi, J. M. Bravo-San Pedro, F. Madeo and G. Kroemer, *Cell Metab.*, 2015, **21**, 805–821.